Available online at www.sciencedirect.com
ScienceDirect
Polymer 48 (2007) 841–848
polymer
www.elsevier.com/locate/polymer

Nanoindentation-induced delamination of submicron polymeric coatings

Kebin Geng [a], Fuqian Yang [a,*], Thad Druffel [b], Eric A. Grulke [a,*]

[a] Department of Chemical and Materials Engineering, University of Kentucky, 359 RGAnderson Hall, Lexington, KY 40506-0503, USA
[b] Optical Dynamics Corporation, 10100 Bluegrass Pkwy, Louisville, KY 40299, USA

Received 23 April 2006; received in revised form 20 July 2006; accepted 21 July 2006
Available online 3 January 2007

Abstract

An elastic model is developed to estimate the interfacial strength between a submicron surface coating and a compliant substrate. The analysis uses a shear-lag model and assumes the plane-stress state in the surface coating. The critical indentation load for the indentation-induced delamination of the coating from the substrate increases with the third power of the indentation depth and is a linear function of the reciprocal of the coating thickness. The indentation-induced delamination of SR399 ultrathin surface coatings over acrylic substrate has been evaluated, using the nanonindentation technique for coating thicknesses of 47, 125, 220 and 3000 nm. For the submicron coatings, the dependence of the critical indentation load on the coating thickness supports the elastic model. The interfacial strength is found to be 46.9 MPa. In contrast, the polymeric coating of 3000 nm displays multiple ''excursions'' in the loading curve, and the critical indentation load is a linear function of the indentation depth.

Keywords: Ultrathin polymeric coating; Nanoindentation; Interfacial strength

1. Introduction

Surface coatings have been widely used in different engineering applications, including scratch-resisting coatings, passivation layers in semiconductor chips and packages, and ceramic thermal barrier coatings for advanced gas turbine engine. For example, a scratch-resistant lens coating can improve the longevity of plastic eyeglass lenses, and multilayered nanoscale coatings with unique optical properties can be constructed to improve optical performance. Surface damage and interfacial failure may affect the performance of coating systems and limit the reliability of devices. Thus, reliable characterization of interfacial strength is critical to the improvement of adhesive properties and to the control of quality in multilayer structure and devices. Accurate and rapid methods for the characterization of submicron coatings would be particularly useful to accelerate product development, to improve product design, and to ensure quality control.

Different techniques have been developed to evaluate the interfacial strength of surface coating, such as blister test [1–3], residual stress-driven delamination test [4], scratch test [5–8] and indentation test [9–15]. The scratch test may be the most popular technique for qualitatively determining the adhesion of various coatings, although it may not provide an absolute measurement of the interfacial strength for the coating–substrate interface [16]. Both the blister test and the residual stress-driven delamination test require complicated sample preparation and are often limited to surface coatings with poor adhesion [12] (i.e. no surface cracking occurs during test).

The indentation-induced delamination of a coating from a substrate is initiated by pushing a rigid indenter into the coating. In some indentations, significant deformation is created only in the coating, while in others, plastic deformation is also introduced in the substrate. There have been reports on the change in the slope and the discontinuity in the load-displacement curves, which is referred to as the ''pop-in''

* Corresponding authors. Tel.: +1 859 257 8028; fax: +1 859 323 1929.
E-mail addresses: fyang0@engr.uky.edu (F. Yang), egrulke@engr.uky.edu (E.A. Grulke).

0032-3861/$ - see front matter © 2006 Elsevier Ltd. All rights reserved.
doi:10.1016/j.polymer.2006.07.075

event or sudden displacement excursion. The occurrence of the ''pop-in'' phenomenon could be related to the phase transition or the indentation-induced delamination. Previous studies of indentation-induced delamination focused on the relation between the indentation load and the delamination size. Chiang et al. [17] evaluated the interfacial strength between a surface coating and a substrate using a Vickers indenter; they suggested that the indentation deformation compressed the coating, leading to the delamination of the coating from the substrate. Using the theory of linear fracture, Evans and Hutchinson [18], Marshall and Evans [11], and Rossington et al. [19] studied the propagation of an interfacial crack to determine the resistance to interfacial delamination. Considering the indentation-induced elastoplastic deformation in a coating, Matthewson [10] proposed that the radial displacement caused by the indentation introduces a shear stress at the interface, which causes the initiation and propagation of adhesive failure. Ritter et al. [20] developed a simple model for calculating the fracture energy based on the dependence of the delamination size on the indentation load. Extending the analysis developed by Marshall and Evans [11], Kriese et al. [16] considered the indentation-induced delamination of a multilayer structure and evaluated the effect of the multilayer structure on the fracture toughness. Vlassak et al. [12] developed a microwedge technique to measure the adhesion of brittle films to ductile films and obtained the fracture toughness as a function of the width of the delamination region.

In general, the indentation-induced interfacial crack propagates in both the loading and the unloading processes. It is very difficult if not impossible to determine *exactly* the size of the delamination zone. This is particularly true for non-brittle, elastic materials that may partially recoil after a delamination event. Thus, it would be useful to determine the interfacial strength from the indentation loading–unloading curve. Based on the shear-lag model, Dehm et al. [13] developed an approximate elastic model for the estimation of the interfacial yield strength of a metal film on a ceramic substrate using a conical indenter, in which they neglected the effect of the deformation in the substrate and assumed that the contact between the film and the substrate was frictionless directly under the indentation. Extending the approach given by Dehm et al. [13] to the indentation of polymeric thin films of poly(methyl methacrylate), polystyrene and high impact polystyrene on a glass substrate using a flat-ended cylindrical indenter, Lu and Shinozaki [9] obtained a critical interfacial shear strength using the Tresca yield criterion. However, there are few studies on the indentation-induced delamination of a submicron polymeric coating on a polymeric substrate with similar elastic properties, which likely displays different behavior from soft coatings on hard substrates.

Studies on thin polymeric films have provided a variety of fascinating and as yet unexplained observations [21], which may be determined by the volume fraction of an interfacial region [22]. A well known phenomenon is the reduction in the glass–rubbery transition temperature (T_g) typically for polystyrene [23–26], which is likely due to the size effect on the equilibrium state of the polymer chains in submicron coatings [23]. Using the nanobubble inflation test, O'Connell and McKenna [27] recently examined the viscoelastic properties of ultrathin polymer films of poly(vinyl acetate) (PVAc). They reported that the rubbery compliance for the thin film of 27.5 nm in thickness is smaller by a factor of about 320 compared to the bulk material [27], although the mechanism is not understood.

Measurement of the mechanical properties of polymer surfaces is likely to provide an insight into the effects of surface interaction and enables us to evaluate the physical processes controlling the physical behavior of thin polymeric films at the micro- and nano-scales. In principle, there are two basic approaches in assessing mechanical properties of polymer surfaces: (a) contact mechanics [28–31] and (b) surface relaxation [32,33]. It is the purpose of this work to study the effect of the coating thickness on the nanoindentation-induced delamination of submicron polymeric coatings on polymeric substrate. A quantitative evaluation of the interfacial strength is described. The indentation-induced delamination is analyzed, relating the indentation load at the excursion in the loading curve to the critical interfacial shear stress at which the delamination initiates.

2. Analysis of the indentation-induced delamination

Consider a conical indenter being pushed into a bilayer structure as shown in Fig. 1. The bilayer structure consists of a thin film coating of thickness h and a half-space substrate. A cylindrical coordinate system is used to describe the deformation of the system, in which the origin of the coordinate

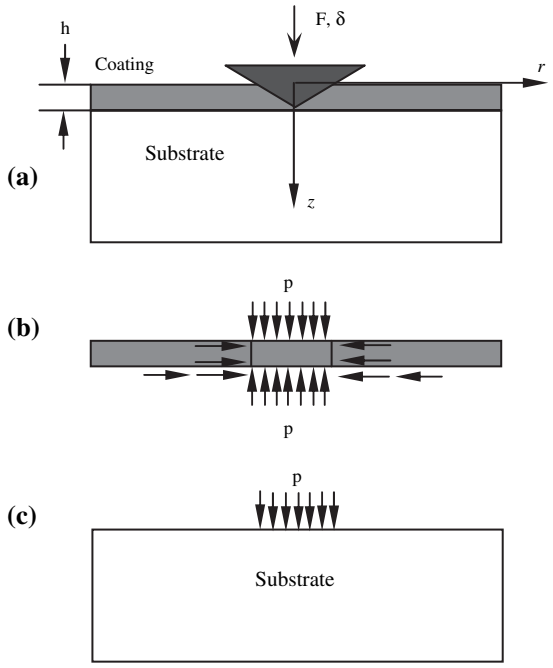

Fig. 1. Schematic of the shear-lag model for the indentation-induced delamination: (a) indentation of a bilayer structure consisting of a surface coating and a substrate, (b) stress distribution in the coating and (c) transfer of the indentation load to the substrate.

system is at the center of the contact zone between the indenter and the surface of the coating and the z-axis is parallel to the loading direction. During the indentation, material is pushed away from the indenter and stresses are created in both the thin film and the substrate. The radial stress in the coating increases with the increase in the indentation depth and eventually causes the delamination of the surface coating from the substrate. As suggested by Dehm et al. [13], the deformation along the radial direction is limited by the ability of the interface to support the radial stress and the transfer of the radial stress can be described by a shear-lag model as shown in Fig. 1. The delamination is controlled by the interfacial strength between the film and the substrate. Based on the analysis used by Dehm et al. [13], we assume that the contact between the substrate and the coating is frictionless directly under the indentation and the deformation in the coating can be approximated via a depth-independent, i.e. a plane-stress state so that

$$\sigma_{ij}^{c}(r,z)=\delta_{ij}\sigma_{ij}^{c}(r)\quad i,j=r,\theta,z\qquad \text{for } r<a \tag{1}$$

where σ_{ij}^{c} are the components of the stress tensor, the superscript c represents the coating, δ_{ij} denotes the Kronecker delta with no summation implied in the equation, and a is the contact radius. In general, the relation between the contact radius, a, and the indentation depth, δ, can be expressed as

$$a=\alpha\delta\tan\theta \tag{2}$$

where α is a constant depending on the system ($\alpha=2/\pi$ for the indentation of an elastic half-space [28,34] and $\alpha=3/2$ for the indentation of an incompressible elastic thin film over a rigid substrate with the contact radius much larger than the film thickness [35]) and θ is the half of the included angle of the conical indenter.

The equilibrium equation for the deformation of the coating under the simplification of the plane-stress state is

$$\frac{\mathrm{d}^2u_{r}^{c}}{\mathrm{d}r^2}+\frac{1}{r}\frac{\mathrm{d}u_{r}^{c}}{\mathrm{d}r}-\frac{u_{r}^{c}}{r^2}=-\frac{\nu^{c}}{2G^{c}}\frac{\mathrm{d}\sigma_{zz}^{c}}{\mathrm{d}r}\qquad \text{for } r<a \tag{3}$$

where u_{r}^{c} is the radial displacement in the coating, and G^{c} and ν^{c} are the shear modulus and Poisson ratio of the coating, respectively. The integration of Eq. (3) gives

$$u_{r}^{c}(r)=Ar-\frac{\nu^{c}}{2G^{c}}\frac{1}{r}\int_{0}^{r}r\sigma_{zz}^{c}(r)\mathrm{d}r\qquad \text{for } r<a \tag{4}$$

with the constant A to be determined.

The radial displacement in the coating is confined by the adhesion of the coating to the substrate. According to Agarwal and Raj [36], the interfacial shear stress around the contact edge can be approximated in a sinusoidal function as

$$\tau=\tau_{m}\sin\frac{\pi r}{2(a+\zeta)}\qquad \text{for } a-\zeta<r<a+\zeta \tag{5}$$

where τ_{m} is the maximum interfacial stress along the interface. The interfacial shear stress rises to the maximum in the regime of $a-\zeta<r<a+\zeta$, in which 2ζ is the size of the influential zone. Considering the force balance at the contact edge, one obtains

$$\sigma_{rr}(a)=\frac{1}{h}\int_{0}^{a+\zeta}\tau\,\mathrm{d}r=\frac{2(a+\zeta)\tau_{m}}{\pi h} \tag{6}$$

For a small influential zone, $\zeta \ll a$, Eq. (6) gives

$$\sigma_{rr}(a)\approx\frac{2a\tau_{m}}{\pi h} \tag{7}$$

Using Eqs. (4) and (7) and the following equations

$$\lim_{r\to a}\sigma_{zz}^{c}(r)=0 \tag{8}$$

$$\sigma_{rr}^{c}=\frac{2G^{c}}{1-\nu^{c}}\left(\frac{\mathrm{d}u_{r}^{c}}{\mathrm{d}r}+\nu^{c}\frac{u_{r}^{c}}{r}\right) \tag{9}$$

and

$$2\pi\int_{0}^{a}r\sigma_{zz}^{c}(r)\mathrm{d}r=F \tag{10}$$

one obtains

$$\frac{a\tau_{m}}{\pi h}=\frac{G^{c}}{1-\nu^{c}}\left((1+\nu^{c})A+\frac{\nu^{c}(1-\nu^{c})}{4G^{c}}\frac{F}{\pi a^2}\right) \tag{11}$$

where F is the indentation load. Solving A from Eq. (11) and substituting it into Eq. (4), one obtains

$$u_{r}^{c}(r)=\frac{(1-\nu^{c})r}{(1+\nu^{c})G^{c}}\left(\frac{a\tau_{m}}{\pi h}-\frac{\nu^{c}}{4}\frac{F}{\pi a^2}\right)-\frac{\nu^{c}}{2G^{c}}\frac{1}{r}\int_{0}^{r}r\sigma_{zz}^{c}(r)\mathrm{d}r\quad \text{for } r<a \tag{12}$$

which is the radial displacement in the coating as induced by the indentation.

Considering the mass balance, one has

$$u_{r}^{c}(a)=\beta\frac{a^2}{h} \tag{13}$$

Here, β is a constant, which is a function of the mechanical properties of both the coating and the substrate and can be determined by numerical simulation. From Eqs. (2) and (13), there is

$$\frac{F}{\delta^3}=\frac{2\pi\alpha^3G^{c}\tan^3\theta}{\nu^{c}h}\left((1-\nu^{c})\frac{\tau_{m}}{G^{c}}-(1+\nu^{c})\beta\right) \tag{14}$$

At the excursion of the indentation-induced delamination, the maximum shear stress is defined as the ''critical interfacial shear strength'', τ_{cr}. Thus, Eq. (14) can be re-written as

$$\frac{F_{cr}}{\delta_{cr}^3}=\frac{2\pi\alpha^3G^{c}\tan^3\theta}{\nu^{c}h}\left((1-\nu^{c})\frac{\tau_{cr}}{G^{c}}-(1+\nu^{c})\beta\right) \tag{15}$$

where F_{cr} is the critical indentation load and δ_{cr} is the corresponding indentation depth. For the same critical interfacial shear strength and β, the parameter F_{cr}/δ_{cr}^3 is inversely proportional to the thickness of the coating. It should be emphasized that, in deriving Eq. (15) the deformation is approximated as a plane-stress state in the coating and no viscoplastic deformation is taken into account.

Using Eqs. (2), (13) and (15), one obtains the radial displacement in the coating at the edge of the delamination, $\tilde{u}_r^c(a)$, as

$$\tilde{u}_r^c(a) = \frac{\beta\nu^c}{2\pi\alpha G^c \tan\theta}\frac{F_{cr}}{\delta_{cr}}\left((1-\nu^c)\frac{\tau_{cr}}{G^c} - (1+\nu^c)\beta\right)^{-1} \qquad (16)$$

which is proportional to the ratio of the indentation load to the indentation depth at the delamination. In general, less indentation load is required for the initiation of interfacial delamination in a bilayer system with a thinner surface coating. Thus, less deformation at the delamination is created in the bilayer system with thinner surface coating as indicated in Eq. (16).

3. Experimental

The polymeric films of dipentaerythritol pentaacrylate monomer (Sartomer SR399) were spin-coated on acrylic substrates, which were provided by Optical Dynamics Corporation (ODC, Louisville, KY). The acrylic substrate was a typical material for polymeric lens, with a modulus about one-half that of the SR399. The thicknesses of the polymeric coatings were 47, 125, 220 and 3000 nm, measured by a profilometer (Ambios Technology XP-1, Santa Cruz, CA). All of the coatings were cured for 90 s in the presence of CO_2 under UV light from a germicidal lamp having an intensity of 4 mW/cm^2 at 5 cm distance. For the detailed information on the sample preparation and polymerization degree, see the work by Geng et al. [28].

The chemistry of the SR399 coatings and the proprietary substrates provided by the ODC was analyzed by Fourier Transform Infrared Spectroscopy (FTIR) (ThermoNicolet Nexus 470) with a resolution of 4 cm^{-1}. At room temperature, the spectrum of the SR399 coating on a KBr plate was recorded by a transmission method, and the spectrum of the acrylic substrate was recorded by the attenuated total reflection Fourier transform infrared spectroscopy (ATR-FTIR). Fig. 2 shows the characteristic infrared absorptions of the SR399 coating and the acrylic substrate. The carbonyl bond is at 1724–1728 cm^{-1}, and the C–O stretching bond at 1270–1150 cm^{-1} [37]. The intensities of the CH=CH stretching at 1407 cm^{-1} and twisting at 809 cm^{-1} are high in the SR399 coating sample due to the residual double bonds in the typical high functional acrylic polymers [28]. The SR399 coating has similar chemistry to the surface of the acrylic substrate.

The nanoindentation tests were performed in a Hysitron TriboScope (Minneapolis, MN) attached to a Quesant (Agoura Hills, CA) atomic force microscope (AFM). A diamond NorthStar cubic indenter with a nominal tip radius of 40 nm (Minneapolis, MN) was used. Constant loading and unloading rates were used in the indentation tests with the intermediate pause of 2 s between the loading phase and the unloading phase. Both the loading and unloading times were 5 s. The indentation depth and applied load were used to evaluate the indentation-induced delamination of the polymeric coatings.

4. Results and discussion

The nanoindentation tests were carried out using the load-control mode with indentation loads within the range of 400–5000 μN. Constant loading and unloading rates were used with both the loading and unloading times of 5 s. AFM was used to image selected impression marks. Fig. 3 shows a typical AFM image of the impression mark indented over the 125 nm

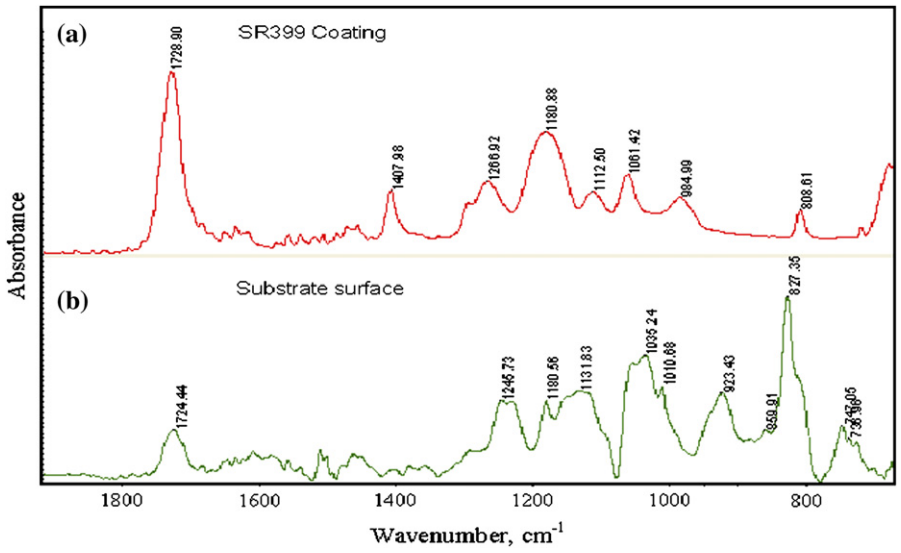

Fig. 2. Characteristic infrared absorptions of the SR399 coating and the acrylic substrate (a) a transmission FTIR spectrum of the SR399 coating and (b) an ATR-FTIR spectrum of the acrylic substrate.

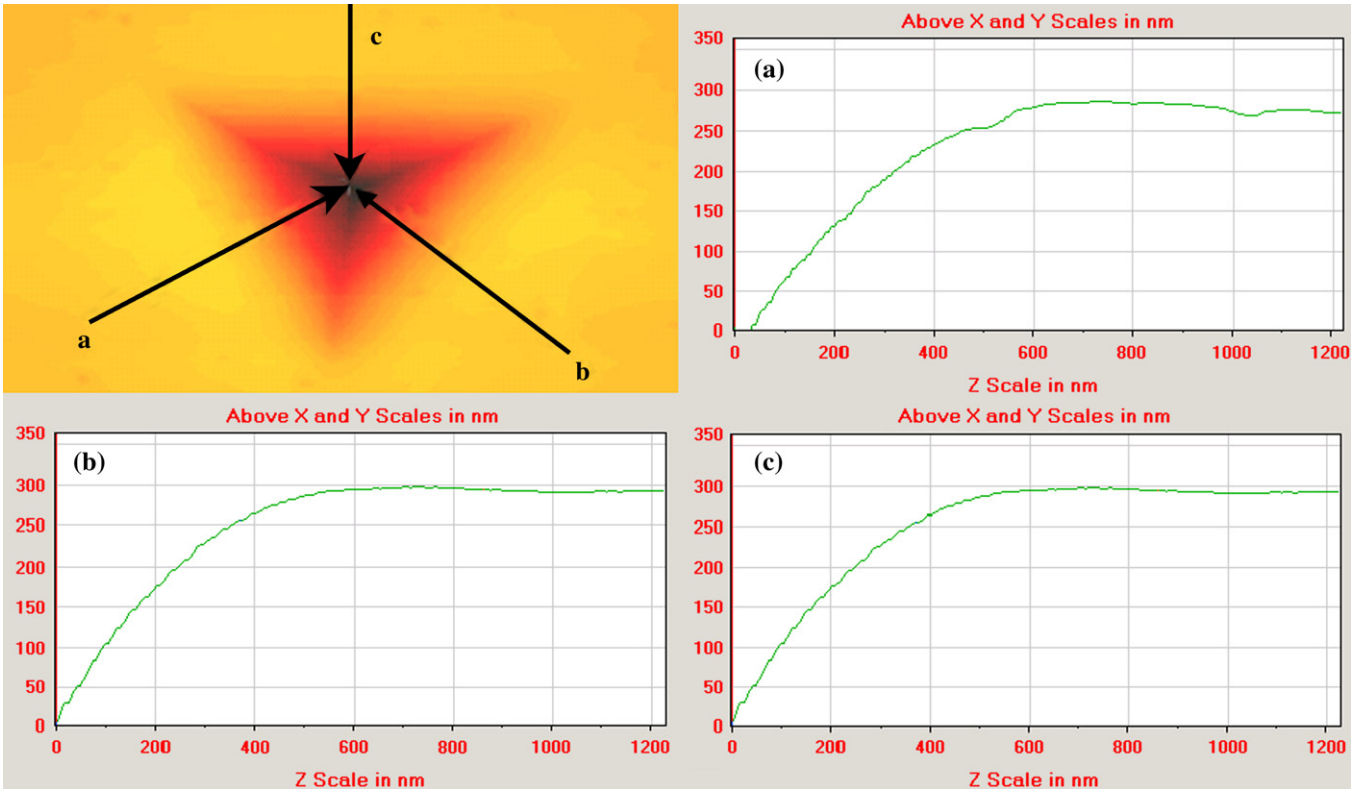

Fig. 3. Typical impression mark and line scans over the indentation profile for the indentation of 125 nm coating at the indentation load of 1200 μN.

coating at the indentation load of 1200 μN and the corresponding morphological profiles of the residual indentation. The indentation profiles are self-similar, and the pile-up around the indentation is observed. The highest pile-up occurs at the region close to the center of each side-contact face, while the lowest pile-up occurs at the singular edges of the indentation due to high stress concentration and less elastic recovery. Smooth impression marks are present and no surface cracks are observed.

A typical example of the loading–unloading curve for the polymeric coatings is shown in Fig. 4, in which the loading–unloading curve for the acrylic substrate is also depicted.

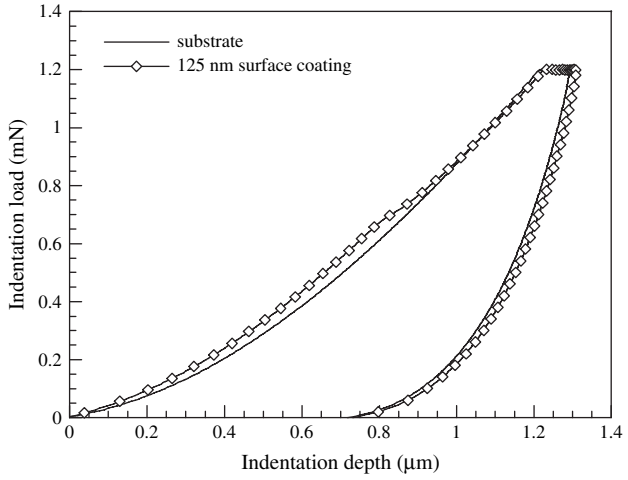

Fig. 4. Typical indentation loading–unloading curves for the indentation of 125 nm surface coating and the acrylic substrate.

There is an excursion during the loading phase near an indentation depth of 800 nm for the 125 nm polymeric coating, clearly differing from the indentation of the substrate only. For the same indentation depth less than 800 nm, larger indentation load was required due to the build up of the stresses in the coating, i.e. more mechanical energy was stored in the coating which eventually led to the delamination of the coating from the substrate. After the delamination, the indentation of the system with the surface coating is similar in appearance to the indentation in the acrylic substrate. This reveals the similar mechanical properties between the surface coating and the acrylic substrate, as expected, since the elastic modulus of the acrylic substrate is about half of that of the surface coating. The contact stiffness as determined from the upper portion of the unloading curve is slightly smaller for the coating system than that for the substrate only. This is due to the layer structure of the coating system, which has less contact stiffness than each individual system similar to the resultant spring constant for the spring system consisting of two springs connected in series. It should be pointed out that there is no excursion for the indentations of the acrylic substrate up to 5000 μN, which strongly suggests that the occurrence of the excursion is associated with the interfacial behavior between the surface coating and the substrate. Based on the impression mark as shown in Fig. 3, it can be concluded that the excursion is likely due to the delamination of the coating from the substrate as suggested in previous discussion.

To evaluate the effect of the loading rate on the indentation-induced delamination, different peak loads were applied to the

indenter. Fig. 5 shows the loading–unloading curves for the indentation of the 125 nm polymeric coating subjected to 5 different peak loads of 400, 800, 1200, 1600 and 2000 μN. The indentation load and indentation depth for the excursion behavior are 696.3 ± 24.1 μN and 829.9 ± 13.2 nm, respectively, independent of the loading rate. Thus, the indentation load for the presence of the excursion is the critical load for the indentation-induced delamination of the 125 nm polymeric coating. Also, there is only one excursion present for indentation loads up to 2000 μN.

In general, the loading stiffness, defined as $dF/d\delta$, is a smooth function of the indentation depth. It is expected that, at the excursion, there will be a change in the loading stiffness representing the occurrence of the indentation-induced delamination. Fig. 6 shows the dependence of the loading stiffness on the indentation depth for three polymeric coatings of 47, 125 and 220 nm. Significant change in the loading stiffness near the excursion is observed for the polymeric coatings of 125 and 220 nm, while less change is found for the polymeric coating of 47 nm. This is due to less deformation required for the initiation of delamination in thin coatings while more deformation is required for thick coatings, i.e. higher indentation load is required to cause delamination in thick coatings, as discussed in the previous section. It should be pointed out that it is very difficult to determine exactly the critical indentation depth for the polymeric coating of 47 nm. The location for the excursion in the 47 nm coating is best estimated from the change in the slope of the loading stiffness-depth curve.

Fig. 7 shows the dependence of the critical indentation load for the initiation of the delamination on the thickness of the polymeric coatings. A linear relation is observed between the parameter, F_{cr}/δ_{cr}^3, and the reciprocal of the coating thickness, which supports Eq. (15). It needs to point out that Eq. (15) is not applicable for $1/h \rightarrow 0$ since the plane-stress state was used in the derivation.

In the previous work [28], we characterized the elastic modulus of ultrathin polymer films of the densely cross-linked submicron dipentaerythritol pentaacrylate (Sartomer SR399)

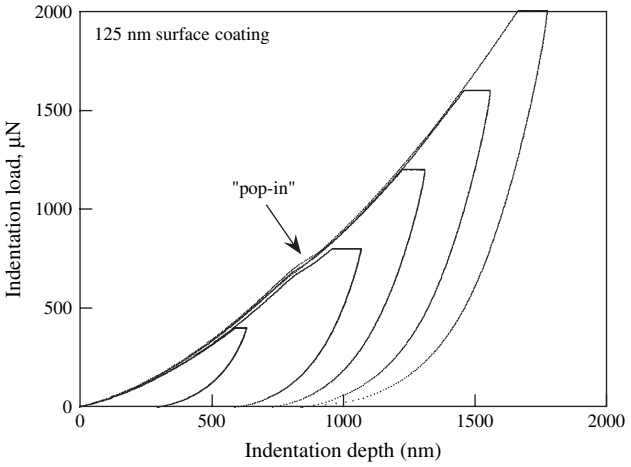

Fig. 5. Effect of the peak indentation load on the "excursion" behavior in the indentation of 125 nm surface coating.

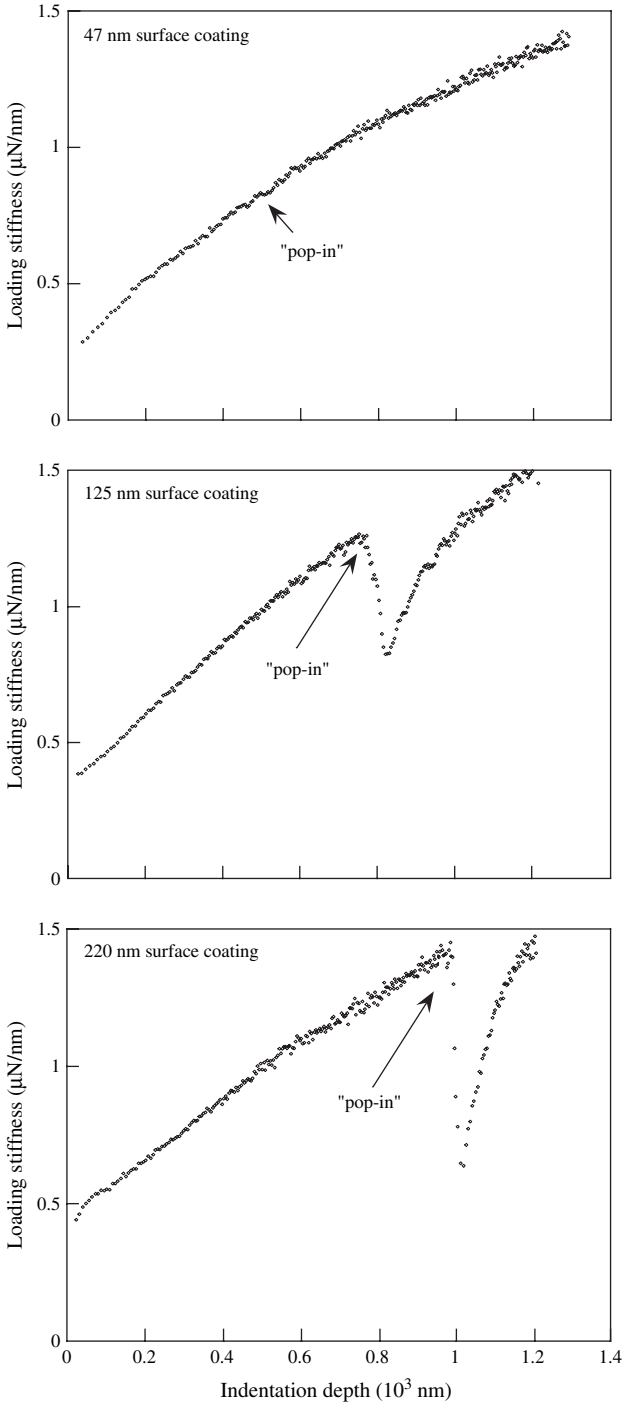

Fig. 6. Dependence of the loading stiffness on the indentation depth for three polymeric coatings of 47, 125 and 220 nm.

with the thicknesses of 47, 125 and 3000 nm. The films were coated on silicon substrate. We did not observe the viscoelastic effect on the reduced contact modulus and the size effect by holding the peak indentation load for 2 s over the indentation period of 12 s. It would be expected that the viscoelastic deformation would not have a strong influence on the indentation deformation in the experimental conditions.

We applied the same technique in the indentations of the polymeric bilayer structures and did not observe the

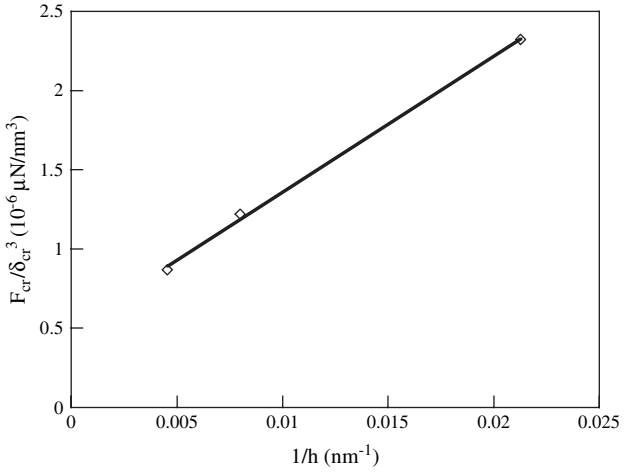

Fig. 7. Dependence of the critical indentation load on the thickness of the polymeric coatings.

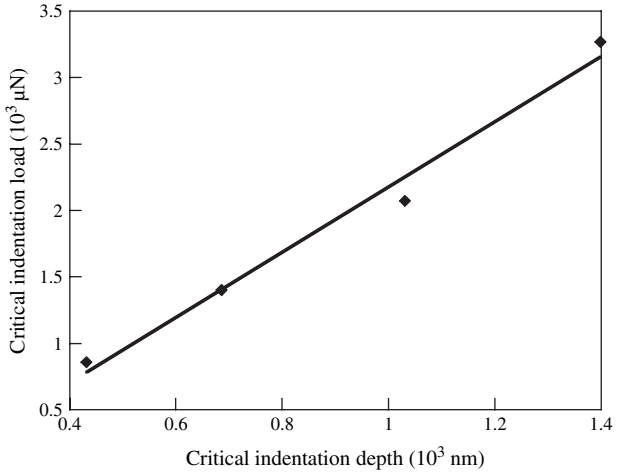

Fig. 9. Correlation between the critical indentation load and the corresponding indentation depth for the indentation-induced delamination in the polymeric coating of 3000 nm.

viscoelastic effect on the reduced contact modulus and the size effect. Using the unloading curves for the indentations of the 3000 nm polymeric coating and assuming the Poisson ratio of the polymeric coatings to be 0.5, we obtain Young's modulus of 4.58 GPa. In general, one can approximate the cubic indenter as a conical indenter with a half included angle of 42.28° (this conical indenter would have the same depth to area ratio as the cubic indenter). On the basis of ultrathin surface coatings over a soft substrate, one can approximate the system as a homogeneous half-space structure and assume $\alpha \approx 2/\pi$ and $\beta \approx 0$. Using Eq. (15) and the slope in Fig. 7, one obtains the interfacial strength of 46.9 MPa.

The indentation-induced delamination was also observed in the indentation of the 3000 nm polymeric coating. Fig. 8 shows the dependence of the loading stiffness on the indentation depth. There are four excursions in the loading curve of the thick coating system. The deepest indentation depth, corresponding to the 4th delamination event, is 1305 nm, about 2/5 time of the coating thickness, suggesting that the stress state in the coating cannot be approximated as a plane-stress state and three-dimensional analysis involving the use of numerical simulation is needed to determine the deformation field. The multiple excursions are likely due to the arrest of the interfacial crack, i.e. the indentation closes the interfacial crack after the onset of the indentation-induced interfacial delamination. There is no enough driving force to cause the further propagation of the interfacial crack. The radial stress along the interface then increases with continuous indentation. Once the radial stress reaches the critical interfacial strength, the interfacial delamination occurs again.

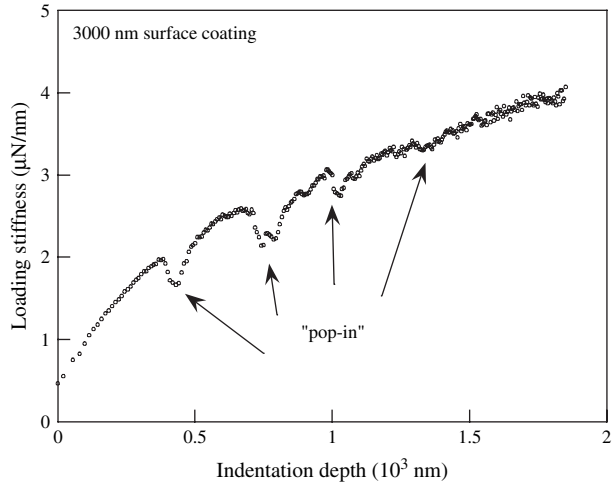

Fig. 8. Dependence of the loading stiffness on the indentation depth for the polymeric coating of 3000 nm at the peak load of 5000 μN.

The dependence of the critical indentation load on the corresponding indentation depth is shown in Fig. 9 for the 3000 nm polymeric coating. Higher indentation load is required to cause the initiation of interfacial delaminations of larger size, as expected. A linear relationship between the critical indentation load and the corresponding indentation depth is obtained. Such a relation provides us a potential mechanism to determine the interfacial strength for thick surface coatings deposited on compliant substrates. However, a new model is needed for evaluating the indentation-induced delamination in thick coatings, which may require the use of numerical simulation.

5. Summary

The indentation-induced delamination provides a unique approach to evaluate the interfacial strength between a surface coating and a compliant substrate. Assuming that the contact radius is much larger than the thickness of the surface coating, we approximate the deformation behavior of the thin surface coating as a plane-stress state. Using a shear-lag model, we have established a relationship between the critical indentation load and the interfacial strength at which interfacial delamination initiates. The ratio of the critical indentation load to the cube of the corresponding indentation depth turns out to be a linear function of the reciprocal of the coating thickness.

The indentation-induced delamination of ultrathin cross-linked polymeric surface coatings over acrylic substrate has been evaluated using the nanonindentation technique over the range of the indentation loads, from 400 μN to 2000 μN for the coating thicknesses of 47, 125 and 220 nm, and over the range of the indentation loads, from 400 μN to 5000 μN for the coating thickness of 3000 nm. For the coatings with the thicknesses of 47, 125 and 220 nm, only one excursion phenomenon is observed in the loading phase, suggesting the arrest of the interfacial crack for deep indentation. The dependence of the critical indentation load on the coating thickness agrees with the proposed model. The interfacial strength is found to be 46.9 MPa. In contrast to the indentation behavior of the submicron coatings, the 3000 nm polymeric coating displays multiple excursions in the loading curve. This is due to the arrest of interfacial crack during the indentation and the increase of the radial stress with further indentation. Once the radial stress reaches the interfacial strength, the interfacial delamination is initiated again. It should be pointed out that a new model is needed for evaluating the indentation-induced delamination in thick coatings, which may require the use of numerical simulation.

Acknowledgements

FY is grateful for support from NSF grant CMS-0508989 and from General Motors Corporation. KG and EG are grateful for support from Optical Dynamic Corporation.

References

[1] Williams ML. J Appl Polym Sci 1970;14:1121.
[2] Bennet SJ, Devries KL, Williams ML. Int J Fract 1974;10:33.
[3] Jensen HM, Thouless MD. Int J Solids Struct 1993;30:779.
[4] Bagchi A, Lucas GE, Suo Z, Evans AG. J Mater Res 1994;9:1734.
[5] Wirasate S, Boerio FJ. J Adhes 2005;81:509.
[6] Huang LY, Lu J, Xu KW. J Phys D Appl Phys 2004;37:2135.
[7] Ramsteiner F, Jaworek T, Weber M, Forster S. Polym Test 2003;22:439.
[8] Zhang SL, Tsou AH, Li JCM. J Appl Polym Sci B Polym Phys 2002;40:1530.
[9] Lu Y, Shinozaki DM. J Mater Sci 2002;37:1283.
[10] Matthewson MJ. Appl Phys Lett 1986;49:1426.
[11] Marshall DB, Evans AG. J Appl Phys 1984;56:2632.
[12] Vlassak JJ, Drory MD, Nix WD. J Mater Res 1997;12:1900.
[13] Dehm G, Rühle M, Conway HD, Raj R. Acta Mater 1997;45:489.
[14] Li M, Palacio ML, Carter CB, Gerberich WW. Thin solid films 2002;416:174.
[15] Li M, Carter CB, Hillmyer MA, Gerberich WW. J Mater Res 2001;16:3378.
[16] Kriese MD, Gerberich WW, Moody NR. J Mater Res 1999;14:3007.
[17] Chiang SS, Marshall DB, Evans AG. J Appl Phys 1982;53:312.
[18] Evans AG, Hutchinson JW. Int J Solids Struc 1984;20:455.
[19] Rossington C, Evans AG, Marshall DB, Khuri-Yakub BT. J Appl Phys 1984;56:2639.
[20] Ritter JE, Lardner TJ, Rosenfeld L, Lin MR. J Appl Phys 1989;66:3626.
[21] Jones RAL, Richards RW. Polymers at surfaces and interfaces. Cambridge: Cambridge University Press; 1999.
[22] Teichroeb JH, Forrest JA. Phys Rev Lett 2003;91:016104.
[23] Alcoutlabi M, McKenna GB. J Phys Condens Matter 2005;17(15):R461.
[24] Reiter G. Eur Phys. J E 2002;8(2):251.
[25] Ellison CJ, Torkelson JM. J Polym Sci Part B Polym Phys 2002;40(24):2745.
[26] Ellison CJ, Torkelson J. Nat Mater 2003;2(10):695.
[27] O'Connell PA, McKenna GB. Science 2005;307(5716):1760.
[28] Geng K, Yang FQ, Druffel T, Grulke EA. Polymer 2005;46:11768.
[29] Fischer H. Macromolecules 2002;35:3592.
[30] Ge S, Pu Y, Zhang W, Rafailovich M, Sokolov J, Buenviaje C, et al. Phys Rev Lett 2000;85:2340.
[31] Oyen ML. J Mater Res 2005;20:2094.
[32] Hutcheson SA, McKenna GB. Phys Rev Lett 2005;94:076103.
[33] Hamdorf M, Johannsmann D. J Chem Phys 2000;112:4262.
[34] Yang FQ. J Polym Sci Part B Polym Phys 2004;42:2513.
[35] Yang FQ. J Phys D Appl Phys 2003;36:50.
[36] Agarwal DC, Raj R. Acta Metall 1989;37:1265.
[37] Ichihashi Y, Henzi P, Bruendel M, Rabus DG, Mohr J. Jpn J Appl Phys 2006;45(4A):2572.